

Enhancing Material Modeling in Additive Manufacturing: Studying a Void Analysis in 3D-Printed Coupon Test Samples by Using Micro-Computed Tomography (μ CT)

Soltansaleki, Ayshan^{1*}, Melenka, Garrett W.^{1*}

¹ Mechanical Engineering, York University, Toronto, Canada

* Corresponding author (gmelenka@yorku.ca)

Keywords: *Fused Filament fabricated composites (FFF), Void Analysis, micro-computed tomography (μ CT)*

ABSTRACT

The utilization of advanced composite materials, like fused filament fabricated composites (FFF), has surged in various industries due to their cost-effective manufacturing process for intricate structures. However, voids and defects during 3D printing can significantly alter material behavior, impacting load-bearing capacity. This study addresses the gap in the literature by analyzing void characteristics in different sample geometries specified by ASTM D638-14 standards. Through PLA filament printing and μ CT imaging, void analysis, including detection, shape, size, and volume fraction, is conducted. Results reveal variations in void morphology and distribution among different sample types, impacting mechanical properties. Samples with uniform void size distribution exhibit reduced stress concentration during tensile tests. Additionally, analysis of void volume fraction suggests a correlation between void density and material strength, with denser structures showing higher ultimate tensile stress. These findings enhance understanding of void effects on composite behavior, aiding future research and applications in additive manufacturing.

1 INTRODUCTION

The usage of advanced composite materials, such as fused filament fabricated composites (FFF), has recently increased in various markets, ranging from aerospace to medical industries. The growing demand can be attributed to the easy and cost-effective manufacturing process for complex geometries and structures. Although using 3D printers is cost-effective and time-efficient, the material behavior is highly sensitive to manufacturing. One crucial parameter affecting the material behavior is the presence of voids and defects during the printing process, even in 100% infill. These voids alter the material behavior under different loading conditions, potentially reducing its ability to tolerate loads compared to the expected capacity. Therefore, the study of these materials under various loading conditions is of paramount importance. [1] Tao *et al.* reviewed the voids of 3D-printed parts using the FFF method. They classified the voids into five groups by their creation method: raster gap voids, Partial neck growth voids, Sub-perimeter voids, Intra-bead voids, and infill voids.[1] These classifications help us categorize each void inside the part and predict the material's behavior around the voids' region. For example, Tronvoll *et al.* used microscopic images along with image processing and statistical analysis to predict the weak plane's behavior of their part for their FEA simulations. [2], [3] However, in their study method, the samples must be destructively sectioned to obtain cross-sectional images for void studies.

Sommacal *et al.* characterized the voids using 3D images of the parts prepared by an X-ray CT machine to prevent the samples from destruction or internal analysis. Their process helped segment and label the voids and categorize them.[4] Many researchers also used μ CT images as a nondestructive method to understand the internal

CANCOM2024 – CANADIAN INTERNATIONAL CONFERENCE ON COMPOSITE MATERIALS

microstructure of 3D-printed parts with reinforced material.[5]–[7] μ CT images are not only used for internal microstructural analysis but also for strain measurement during quasi-static and dynamic loading situations. For example, the late strain measurement method, digital volume correlation (DVC), also uses μ CT images to calculate the strain map inside the test specimen without destroying the part.[5] Recently, the application of the DVC method has increased in the field of 3D-printed composite object studies. Accordingly, voids studies' effects on composite object behavior are undeniable.

Moreover, detecting or predicting the voids' shapes, location and distribution inside the object provides the opportunity for exact FEA simulation of the objects. For example, Ying *et al.* [8] used 2D X-ray images to reconstruct a 3D model of their specimens in order to simulate their heterogeneous material for finite element analysis. In this regard, heterogeneous geometries, like 3D-printed objects, can be modelled precisely.

The Computer-Aided Design (CAD) model of the 3D-printed object in an experiment has been chosen mostly based on the suggested geometry type by American Society for Testing and Materials (ASTM) standards and the experiment's instrument limits. Also, different types of specimen geometry have different void configurations during the manufacturing process. Generalizing the results of various studies on various standard geometries cannot effectively predict the overall behavior of complex geometries. This is the literature gap that this study tries to cover. For this purpose, all types of samples in ASTM D638-14 were printed by PLA filament and studied the void analysis, which means the void detection, shape, size, and volume fraction. Each of these parameters has specific effects on the object's mechanical behavior. These parameters can be applied to the complex geometry simulation in FEA. For example, in complex 3D-printed geometries, we can detect different types of voids from extracted G-Code. Since the type of raster changed, the configured inside voids are also changed. According to Monaldo *et al.*, the provided multiscale simulation results to model the damage and plasticity of specific configurations of rasters in 3D-printed material agree with experimental stress and strain results with an error of 3.7%. [9] This means that if we have multiscale simulations of different types of voids models, we can predict the precise behavior-voids models, and we can predict the precise behavior of the complex 3D-printed objects by using just the G-Code geometry. However, the voids' geometries extracted by G-code are not the same with the voids' geometries extracted by G-code are not the same as the reality after manufacturing. Therefore, the initial aim of this study is to detect the real voids' type after the printing process. Then, the multiscale simulation process will be applied to the FEA model for future study.[10]

2 Method

Based on the introduction part, analyzing the voids inside the 3D-printed object has a valuable effect on predicting the behavior of the objects. For this purpose, initially, all solid model types of ASTM D638-14 [11] Samples were generated using the CAD module (DesignModular) of ANSYS Workbench 2023 R1, provided by CMC microsystem, and G-code was generated using PrusaSlicer 2.6.0. Then, they were printed by a 3D printer and scanned with a micro-computed tomography (μ CT) instrument. After gathering the μ CT scans, the cross-sectional images and preprocessing methods, like reducing noises on the images, were done based on Timpano's *et al.* study. [12]Then, when the images were prepared for void analysis, the shapes, dimensions, and areas of all the voids were calculated.

2.1 3D Printing

Samples type I, II, III, IV, and V (Figure 1a) were printed with red PLA at 210°C by Prusa i3 MK2, Czech Republic, with a bed temperature of 60°C. Printing Parameters are available in Table 1. The 90° orientation for rasters has been chosen to make a stronger part based on studies by Hernandez *et al.* [13]. Besides, since the number of perimeters was 2, we expected that the sub-perimeter voids would be present in the part. Besides, all the raster (the pattern of parallel lines) are in the same direction in each printing layer (thin layers of material that are deposited one upon the other to form the final object). In this case, we expected to see the intra-bead voids (voids within the structure of individual printed layers during the additive manufacturing process[10]). These voids are shown in Figure 1(b).

CANCOM2024 – CANADIAN INTERNATIONAL CONFERENCE ON COMPOSITE MATERIALS

Table 1: 3D Printing Parameters

Infill	100%	Nozzle size	0.4 mm
Layer Height	0.2 mm	Nozzle temperature	210 °C

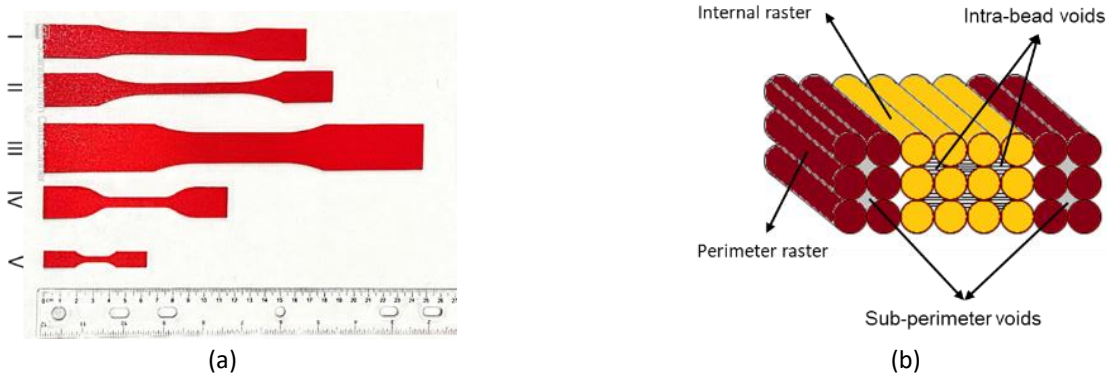


Figure 1: (a) All types of sample geometry in ASTM D638-14, (b) Voids' type by different raster types in the 3D-print process

2.2 Micro Computed tomography (μ CT)

Scanning of the parts had been done by Skyscan 1272 μ CT scanner, Bruker, Belgium. This machine radiates an X-ray beam from a source to the objects, and the shadow of parts is detected on the detector as an image. The objects rotate gradually, and the detector collects several images for each rotational step. The μ CT software provides an average of these few images and saves them into the computer. Based on the distance of objects to the source and detectors, the binning of the images is defined. Also, the machine has different filters to increase or decrease the intensity of the x-ray beam. The schematic diagram of the μ CT is shown in Figure 2 (a). Figure 2 (b) shows μ CT image for the front and side views of sample Type I. The scanning parameters are shown in Table 2. Since there is a dimensional limit in the μ CT machine, the gauge length of each sample was cut by a diamond wire saw.

Once scanning is done, NRecon software (version 1.7.1.0, Bruker, Belgium) reconstructs the cross-sectional images. For reducing ring artifacts, the correction number was chosen as 15. The 3D view of all types of standard geometries (Figure 3) had been done by MATLAB 2023 in Volume Viewer. However, before 3D views of the part, some preprocessing is applied to raw images. When the cross-sectional images are reconstructed, some noises around the detected object must be eliminated before processing. In this case, the "filter" function filtered the images with a 2000 value. Then, the colormap intensity of the images was adjusted. The "Canny" edge detector function is applied to images in the next step. The 'disk' option with value 9 used the morphological operation to enhance the void shapes. Also, binarizing the images is essential for void analysis, and the value for binarizing was 0.498.[12]

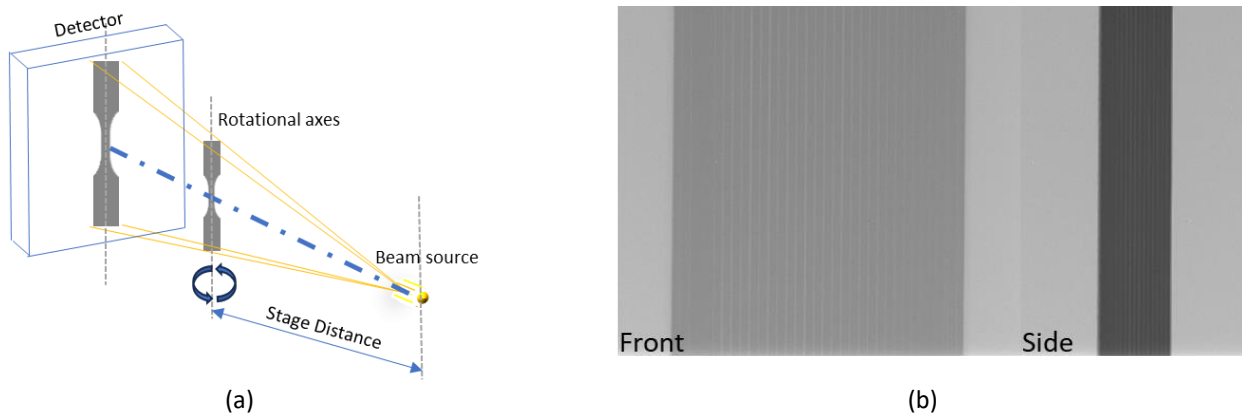


Figure 2: (a) Schematic diagram to show how μ CT works, (b) μ CT image for Front view and side view of sample Type I

CANCOM2024 – CANADIAN INTERNATIONAL CONFERENCE ON COMPOSITE MATERIALS

Table 2: Scanning Parameters for all Types of geometries in ASTM D638-14 standard

	Type I	Type II	Type III	Type IV	Type V
Camera Pixel Size (um)	10	5	5	5	5.4
Resolution (pixel)	2452×2452	2452×2452	4688×4688	2452×2452	2452×2452
Field of View (mm)	24.52*24.52	12.26*12.26	24.52*24.52	12.26*12.26	13.24*13.24
Camera binning	Source Voltage (kV)	Source Current (μA)	Rotation Step (deg)	Flat Field Correction	Filter
2x2	60	125	0.3	On	Al 0.5 mm

2.3 Void Analysis

The volumetric graphic is provided for the next step, and the volumetric image is binarized based on the image threshold. Then, each element is labelled for the connected component, and the “regionprops” function provides the intended parameters, like the void’s area, centroid, etc. This algorithm is defined by closed regions in the images. Once void detection is done, useful information will be provided on studying the void’s features and properties. In this study, one crucial parameter for voids study (like Hernandez *et al.* [13]) is looking for the volume fraction of voids in each sample. The volume fraction V_v of a void is calculated in a mixture by Equation (1).

$$V_v = \frac{V_{voids}}{V_{total}} \quad (1)$$

V_{voids} is the volume of voids, and V_{total} is the total volume of the object. The voids’ volume was calculated by counting the number of detected voids’ pixels. Since each image has a specific correspondent pixel size, the area of each void can be calculated by counting the number of pixels in the binarized image and multiplying it by the image’s pixel size. In Figure 4 the variation of this parameter is shown in different types of sample shapes.


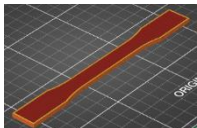
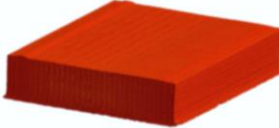
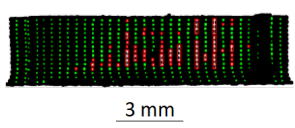

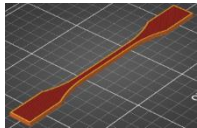
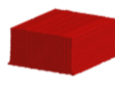
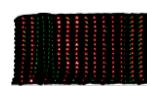

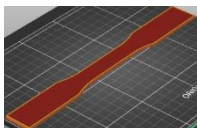



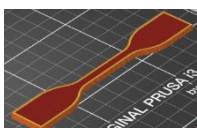
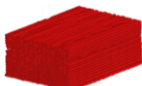


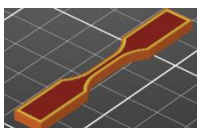
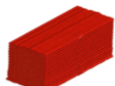
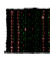
	Real 3D-Printed	G-code Geometry	μCT Volumetric Image	Voids in Mid-Section
Type I				 3 mm
Type II				 3 mm
Type III				 3 mm
Type IV				 3 mm
Type V				 3 mm

Figure 3. All coupon test type geometry in ASTM D638-14 standard

2.4 Results and Discussion

2.4.1 Void Shape Analysis and Distribution

Figure 3 depicts the first column as real pictures, the second as G-codes, the third as MATLAB 3D reconstructions, and the fourth as 2D void detection for all sample types. The last column classifies the voids into two large and small sizes with a threshold size of 30 Pixels (if the region properties of the area are less than 30 pixels, it counts as a small-size void; Otherwise, it is a large void). This number for size has been chosen as 25% to 30% above the minimum average of detected void area. In this case, all the voids can be separated for all types with the same number. The minimum average is related to types I and V, which are 22.5 and 25 Pixels. Large voids are detected as red colour boxes, and small ones are detected as green colour boxes. This threshold has been chosen uniquely to classify all the voids inside all sample types for comparison. However, this threshold specifically distinguishes the voids model based on Hernandez *et al.* in Type V [13] studies. In Type V, the red boxes mostly detect the sub-perimeter voids in two successive rows of raster located vertically on the two sides of cross sections. This means that defining many perimeters in slicer software increases the large voids inside the Type V.

Also, comparing the ratio of each void to the whole volume of the object provides a good sense of geometrical effects on the void type. This variation is shown in Figure 4 a quantitative assessment of void morphology and distribution (Figure 3, Figure 4) reveals that Type IV exhibits the highest porosity ratio to the geometry compared to other samples. Although Type IV is recognized as a type with a higher porosity area, since the number of detected voids is less than others, it can be predicted that it has larger areas. This is because the small voids are connected to each other and provide a big void instead of several small ones. These connected voids can be seen in Figure 3. On the other hand, samples Types I, II, & V have a more uniform void size distribution, reducing stress concentration during tensile tests compared to larger voids. [14] In this case, Sample Type I, II, and V are the best options for tensile tests if a lack of thickness is required. Additionally, it would be good to remember that all the samples were printed simultaneously, so the voids' structures would not vary from sample to sample under the influence of the printing process.

2.4.2 Void Volume Fraction Analysis

Based on Figure 5 the analysis of void volume fraction confirms that Type IV possesses the largest volume occupied by voids. Conversely, Type V exhibits the lowest void volume fraction, indicating a denser structure with a smaller proportion of voids compared to other samples. Since the less void volume fraction in 3D printed parts predicts stronger material [13], [15], it has been predicted that samples Type I and Type V have higher ultimate tensile stress because of the lower void volume fraction. In this regard, Type I and V will be targeted testing geometry for future study of this research to reach the tensile mechanical properties from experimental tests, which will lead us to provide more precise FEA analysis.

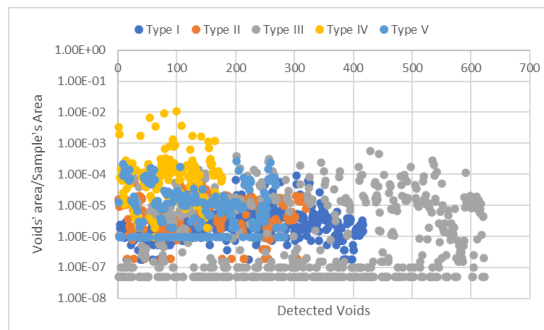


Figure 4: The logarithmic scale of the detected voids' area ratio to the total geometry area for each ASTM D638-14 standard type

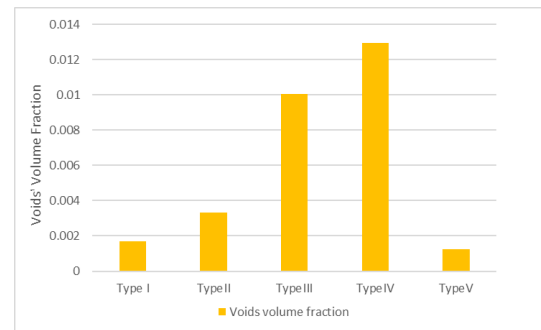


Figure 5: Volume fraction V_v variation for all ASTM D638-14 standard samples

3 Conclusion

In sum, in 3D printed parts, despite the 100% infill printing parameter, the presence of voids is unavoidable. In this case, real voids study analysis provides beneficial material and geometry modelling results. In this study, the presence of the void in different types of test samples (ASTM D638-14) has been studied. All the samples have been printed simultaneously, and the voids study has been done by μ CT images. The study shows that samples Type I and Type V are the best options for the tensile test experiments if there is a limit for the thickness of the coupons. Moreover, based on the literature, it has been predicted that samples Type I and V might have higher ultimate tensile stress because of less void volume fraction and denser structure.

4 REFERENCES

- [1] Y. Tao *et al.*, “A review on voids of 3D printed parts by fused filament fabrication,” *J. Mater. Res. Technol.*, vol. 15, pp. 4860–4879, 2021.
- [2] S. A. Tronvoll, “The effects of voids on structural properties of fused deposition modelled parts: a probabilistic approach,” *Int. J. Adv. Manuf. Technol.*, vol. 97, no. 9–12, pp. 3607–3618, 2018.
- [3] S. A. Tronvoll, “A new method for assessing anisotropy in fused deposition modeled parts using computed tomography data,” *Int. J. Adv. Manuf. Technol.*, vol. 105, no. 1–4, pp. 47–65, 2019.
- [4] S. Sommacal, “Detailed void characterisation by X-ray computed tomography of material extrusion 3D printed carbon fibre/PEEK,” *Compos. Struct.*, vol. 308, no. December 2022, p. 116635, 2023.
- [5] A. Goyal, “Mapping internal strain fields of fused filament fabrication metal filled polylactic acid structure using digital volume correlation,” *J. Compos. Mater.*, 2023.
- [6] X. Wang, “Effect of porosity on mechanical properties of 3D printed polymers: Micromechanical modeling based on X-ray computed tomography analysis,” *Polymers (Basel)*, vol. 11, no. 7, 2019.
- [7] J. Holmes, “Digital image and volume correlation for deformation and damage characterisation of fibre-reinforced composites: A review,” *Compos. Struct.*, vol. 315, p. 116994, Jul. 2023.
- [8] H. Ying, “Heterogeneous Finite-Element Modeling of the Dynamic Complex Modulus Test of Asphalt Mixture Using X-ray Computed Tomography,” *J. Mater. Civ. Eng.*, vol. 26, no. 9, pp. 1–7, 2014.
- [9] E. Monaldo, “Modelling of damage and plasticity phenomena in 3D printed materials via a multiscale approach,” *Eur. J. Mech. A/Solids*, vol. 103, p. 105140, 2024.
- [10] E. A. Papon, “Tensile properties, void contents, dispersion and fracture behaviour of 3D printed carbon nanofiber reinforced composites,” *J. Reinf. Plast. Compos.*, vol. 37, no. 6, pp. 381–395, 2018.
- [11] P. Materials, “Standard Test Method for Tensile Properties of Plastics 1,” no. January 2004, pp. 1–15, 2006.
- [12] C. S. Timpano, “Digital volume correlation analysis of polylactic acid based fused filament fabrication printed composites,” *J. Compos. Mater.*, vol. 55, no. 25, pp. 3699–3717, Oct. 2021.
- [13] A. Hernandez-Contreras, “Extended CT void analysis in FDM additive manufacturing components,” *Materials (Basel)*, vol. 13, no. 17, 2020.
- [14] V. S. Kravets, “Deformation of an Isotropic Plate with Periodic System of Curvilinear Holes and Plasticity Bands,” *Mater. Sci.*, vol. 56, no. 3, pp. 301–309, 2020.
- [15] K. Khanafer, “Investigation of the Mechanical Characteristics of Metal 3D Printing at Different Build Orientation and Directions,” *J. Eng. Mater. Technol.*, vol. 146, no. 3, Jul. 2024.